Published in final edited form as:
Magn Reson Med. 2008 October ; 60(4): 790–795. doi:10.1002/mrm.21715.

The Age Dependence of Regional Proton Metabolites T_2 Relaxation Times in the Human Brain at 3 Tesla

Ivan I. Kirov, **Lazar Fleysher**, **Roman Fleysher**, **Vishal Patil**, **Songtao Liu**, and **Oded Gonen**
Department of Radiology, New York University School of Medicine, New York, NY, USA

Abstract

Although recent studies indicate that use of a single global transverse relaxation time, T_2, per metabolite is sufficient for better than ±10% quantification precision at intermediate and short echo-time spectroscopy in young adults, the age-dependence of this finding is unknown. Consequently, the age effect on regional brain choline (Cho), creatine (Cr) and *N*-acetylaspartate (NAA) T_2s was examined in four age groups using 3D (4 slices, 80 voxels 1 cm^3 each) proton MR spectroscopy in an optimized two-point protocol. Metabolite T_2s were estimated in each voxel and in ten gray and white matter (GM, WM) structures in 20 healthy subjects: four adolescents (13±1 years old), eight young adults (26±1); two middle-aged (51±6) and six elderly (74±3). The results reveal that T_2s in GM (average±standard error of the mean) of adolescents (NAA: 301±30, Cr: 162±7, Cho: 263±7 ms), young adults (NAA: 269±7, Cr: 156±7, Cho: 226±9 ms) and elderly (NAA: 259±13, Cr: 154±8, Cho: 229±14 ms), were 30%, 16% and 10% shorter than in WM, yielding mean global T_2s of NAA: 343, Cr: 172, and Cho: 248 ms. The elderly NAA, Cr and Cho T_2s were 12%, 6% and 10% shorter than the adolescents', a change of under 1 ms/year assuming a linear decline with age. Formulae for T_2 age-correction for higher quantification precision are provided.

Keywords

Aging; Brain; High-field; MR spectroscopy; Relaxation time

INTRODUCTION

Proton MR spectroscopy (^{1}H-MRS) is often used to add metabolic specificity to clinical MRI (1). Unlike MRI, where anatomy or contrast is evaluated visually, ^{1}H-MRS requires to account for parameters that affect its quantitative assessment. While instrumental factors, *e.g.*, static and radio-frequency field inhomogeneities can be handled by field mapping (2), line fitting (3,4) and internal water referencing (5,6), the molecular environment factors require knowledge of the local longitudinal, T_1, and transverse, T_2, relaxation times (7). Although quantification can be made insensitive to T_1 variations at long recycle-times, $TR \gg T_1$, T_2 weighting is minimal only at very short echo-times, $TE \ll T_2$. Since intermediate- and long-*TE* spectra are often favored due to their flatter baseline, reduced lipid contamination and simplified peak structure (7), their reliable quantification depends on a good estimate of metabolic T_2s (8,9).

Unfortunately, the single voxel studies used in the past to obtain these T_2s suffered two main limitations: First, to achieve sufficient signal to noise ratio (SNR) in a 7 – 10 minute

Corresponding Author/Reprints requests: Oded Gonen, PhD., Department of Radiology, New York University School of Medicine, 650 First Avenue, New York, New York 10016, Telephone/FAX: (212) 263-3532/(212) 263-7541, E-mail: oded.gonen@med.nyu.edu.

acquisition, even at the higher 3 T clinical field, requires 3.5 – 8 cm^3 voxels, leading to white and gray matter (WM, GM) partial volume effects. Second, each different region requires separate acquisitions, limiting the number that can be studied in a single session. This forced two implicit assumptions on quantitative ^{1}H-MRS: *(i)* That the same global T_2s are good for the entire brain; and *(ii)* that all healthy subjects share the same T_2 values.

Fortunately, multivoxel methods used recently to address these limitations with better spatial resolution and coverage have substantiated both assumptions in controls (8,9), showing that they lead to under ±10% quantification bias (8). Although ^{1}H-MRS is used across all ages, these studies focused on young adults, leaving unknown any age effects on regional T_2s of *N*-acetylaspartate (NAA), total creatine (Cr) and choline (Cho). To test the hypothesis that a global T_2 per metabolite may still apply to controls of all ages we measured the brain's regional T_2 distributions at 3 T in healthy adolescents, young adults, middle aged and elderly subjects at 1 cm^3 spatial resolution. Extensive brain coverage was obtained with three-dimensional (3D) ^{1}H-MRS in a precision-optimized two-point protocol (10,11).

MATERIALS AND METHODS

Human Subjects

Twenty healthy volunteers with no history of neurological conditions were recruited for this study: Four adolescents (3 female), 13±1years old (yo); eight young adults (4 women), 26±1 yo, two middle-aged (1 woman), 51±6 yo; and six elderly (3 women), 74±3 yo. Healthy status in the elderly was established based on a Mini Mental State Examination (MMSE) for general cognitive performance (12); Global Deterioration Scale (GDS) to exclude cognition related functional issues (13); Brief Cognitive Rating Scale (BCRS) interview for memory performance and global functioning (14); and a physical exam with screening MRI as well as blood work-up for general medical conditions. For the younger cohorts, "healthy" status was established based on negative answers to a questionnaire detailing 28 disqualifying neurological conditions before the study and an "unremarkable" MRI confirmed by a neuroradiologist after the scan. Participants or their guardians gave IRB-approved written informed consent.

MR Data Acquisition

All experiments were done in a 3 T Magnetom Trio (Siemens AG, Erlangen, Germany) with a circularly-polarized transmit-receive head coil (TEM3000 MRI Instruments, Minneapolis, MN). The ^{1}H-MRS volume-of-interest (VOI) was image-guided over axial, sagittal and coronal T_1-weighted spin-echo (*TE*/*TR*=7.3/600 ms) MRI acquired at 240×240 mm^2 field-of-view (FOV), 256×256 matrix and 5 mm thick slices, as shown in Figs. 1 and 2. Our chemical-shift imaging (CSI) based auto-shim produced consistent full-width at half maximum (FWHM) whole-head water linewidth of 27±4 Hz (15). The 10 cm anterior-posterior (AP) ×8 cm left-right (LR) ×4 cm inferior-superior (IS) =320 cm^3 VOI was excited using PRESS (*TR*=1260 ms, *TE* see below) with water suppression enhanced through T1 effects (16,17). The VOI was encoded using two-slab second-order Hadamard spectroscopic imaging into 4 (IS) slices, each partitioned with 16×16 CSI over a 16×16 cm^2 (AP×LR) FOV, as shown in Figs. 1 and 2, in 11 minutes (18,19). This yielded 320 voxels, a nominal 1 cm^3 each, or approximately 1.12×1.12×1.0=1.25 cm^3 given the FWHM of the point spread function for the uniform 2D phase encoding in the axial planes (19–21). The ^{1}H-MRS signals were acquired with 512 complex points at 500 ms/pt digitization rate for a ±1 kHz acquisition bandwidth with the carrier frequency centered 2.7 ppm upfield from the water resonance, *i.e.*, between the Cr and NAA.

Choice of *TE* and acquisition strategy

The strive for spatial resolution *and* T_2 precision in the noisy MRS experiment makes for a long acquisition. To maximize its efficiency we employed two strategies: 3D ^{1}H-MRS that yields the same SNR/unit-time as single-voxel methods (22) but covers a much larger volume (18); and a two-point T_2 estimation paradigm that optimizes not just the two *TE*s, but also the number of averages (N_1 and N_2) at each, for the best precision/unit-time (11). Given that literature Cho, Cr and NAA T_2s of young adults lie in the 130–260 ms range (8,9), the protocol was tuned for T_2s around T_2^0 = 180 ms, which led to TE_1=35 ms (minimum for our setup), N_1=1 and TE_2 =260 ms (TE_1+1.25×T_2^0), N_2=3 (10,11). The uncertainty in the resultant T_2s remains similar over a −25% to +40% range about T_2^0, as shown in Fig. 2 of reference (8). This strategy led to a 44 minute protocol: Eleven min. at TE_1 and 33 min. at TE_2.

Post Processing and T_2 metabolite Calculation

The MRS data were processed offline using in-house software. Residual water signal was removed in the time domain (23) and the data voxel shifted to align the CSI grid with the NAA VOI. The data was then zero-filled in the axial (CSI-encoded) planes from 16×16 to 256×256, Fourier transforms in the time, AP and LR dimensions and a Hadamard transform along the IS direction followed. No temporal or spatial filters were applied. [Although zero-filling does not add any information content to the raw data, our rationale is that it can increase the effective spatial resolution by providing overlapping voxels, thereby reducing partial volume artifacts (24,25)]. The spectra were automatically corrected for frequency and zero-order phase shifts in reference to the NAA peak in each voxel (18).

The relative levels of NAA, Cr, and Cho in every voxel in the VOI were estimated from their peak areas obtained with the parametric spectral modeling and least-squares optimization method of Soher *et al.* (3), as shown in Fig. 3. This process uses a priori spectral information and includes non-parametric baseline signal components characterization and Lorenz-Gauss lineshape assumption. Analysis of this baseline modeling showed that for spectra with 5 Hz linewidth, the mean errors of the fit are 3.4%, 2.3% and 2.8% for NAA, Cr and Cho (26).

Proton T_2 relaxation times for NAA, Cho and Cr in each voxel were estimated using (8),

$$T_2=(TE_2 - TE_1)/\ln\ (S_1/S_2), \quad [1]$$

where S_1 and S_2 are the metabolite's peak areas at TE_1, and TE_2. Five GM and five WM structures were manually outlined on the MRI, as shown in Figs. 1 and 3 and our software averaged the metabolites' T_2s in all the voxels in the 256×256 T_2 map that fell completely or partially within each. No CSF partial volume correction was made to the estimated metabolite levels since it self-cancels in the S_1 / S_2 ratio of Eq. [1]. Similarly, the small $\mathbf{B_1}$ variations across the VOI will also affect both S_1 and S_2 in Eq. [1] in a multiplicative way since the same pulses are used to acquire both and, therefore, will cancel out. As a result, both the partial volume and the $\mathbf{B_1}$ variations will have some effect on the voxel SNR, and consequently, a minor influence on the precision of the T_2 but not on its accuracy.

RESULTS

Examples of the position of the VOI in the brains and the resultant ^{1}H spectra matrices obtained at the short and long *TE*s from an adolescent and an elderly subject are shown in Figs. 1 and 2. The WM and GM structures outlined for the regional T_2 estimates, are shown

in Figs. 1 and 3, together with sample spectra from adolescents and elderly at both *TE*s. These spectra are overlaid with the fitted model functions comprising NAA, Cho, Cr, glutamate, glutamine, aspartate and lactate at the short, TE_1=35 ms, and just NAA, Cr and Cho at the long TE_2=260 ms. Expanded for detail in Fig. 3, these spectra demonstrate the characteristic SNR, linewidth and overall quality of the fit, from which the T_2s are derived via Eq. [1].

The average NAA, Cr, and Cho SNRs at TE_1, estimated as the peak-height divided by twice the root-mean-square of the noise [see 4.3.14 in (27)], were 40±7.0, 18±5.0 and 15±4.0 [mean±standard deviation (SD)]. All T_2s were corrected for the T_1-weighting incurred by our use of the 1.260 s TR, assuming an average T_1 value of ~1.2 s for each of the three metabolites reported in the literature (28). The T_2s in each of the examined brain region shown in Figs. 1 and 3 in the adolescents, young adults and elderly are compiled in Table 1, and the histograms from all 320 voxels in the VOI of each adolescent and elderly are plotted in Fig. 4. Note the inter-subject T_2 distribution similarities, reflected by the histograms overlap for each metabolite in the two age-extreme cohorts. The GM and WM T_2s means ± standard-error of the mean (SEM) for the three metabolites in each of the four cohorts studied, are plotted versus age in Fig. 5.

The results show that the T_2s (mean±SEM) in the GM of the adolescents (NAA: 301±30, Cr: 162±7, Cho: 263±7 ms), young adults (NAA: 269±7, Cr: 156±7, Cho: 226±9 ms) and elderly (NAA: 259±13, Cr: 154±8, Cho: 229±14 ms), were 30%, 16% and 10% shorter than in their WM. Furthermore, in both GM and WM the T_2s of NAA, Cr and Cho in the elderly were 12%, 6% and 10% shorter than in the same regions in the adolescents. Assuming a linear decline, these represent changes of less than 1 ms/year of aging in each moiety, as shown in Fig. 5.

The spectral fitting software also estimates the metabolites' FWHM linewidth, $\Delta\omega$ in each voxel: 2.91±0.07, 3.16±0.15, 3.31±0.07, 3.33±0.05 Hz (mean±SEM) in the adolescents, young adults, middle-aged and the elderly cohorts. Assuming Lorentzian lineshapes, the corresponding T_2*s ($=1/\pi\Delta\omega$) were 109±4, 101±2, 96±5 and 95±6 ms. Since these $\Delta\omega$–s scale down from the 27±4 Hz FWHM in the 8×10×4 cm^3 VOI approximately as its ratio to the 1×1×1 cm^3 voxel, indicates that macroscopic susceptibility dominates the linewidth, as described by Li *et al.* (29).

DISCUSSION

Although ^{1}H-MRS is also used in pediatric and geriatric populations, all T_2 studies known to us at 3 T to date focused on young adults in their 20–30s (8,9,28,30,31). Yet it is known that over the 60–80 years separating the two age-extreme groups, the human brain undergoes morphologic and physiologic changes that could affect T_2. Of these, atrophy is the best known and easiest to see, *e.g.*, by comparing ventricle and subarachnoid spaces in Fig. 1 versus 2 (32). Since atrophy in normal aging involves neuronal shrinkage, axonal and myelin degeneration (33,34), the resulting increase in the fraction of small neurons and corresponding reduction in their water content may combine to decrease metabolite T_2s. In addition, progressive iron ($^{+3}$Fe) buildup with age (as transferrin, ferritin and hemosiderin) first observed by Hallgren and Sourander (35), especially in the basal ganglia, has shown a strong correlation with T_2* decline (36,37).

These morphological and biochemical age-related changes, motivated us to assess, for the first time, the inter- and intra-subject variability of metabolites' T_2s within and between adolescents, young adults, middle-aged and the elderly. Our aim was to obtain these T_2s and

ascertain if, or at what consequence, can a global value for each still be (conveniently) used for absolute metabolic quantification *anywhere* in the brain of *any* healthy subject.

Indeed, for the purpose of metabolic quantification, this premise is supported by our results. Specifically, the variations in T_2 among the brain structures and tissue type (GM or WM) studied is less than 35% for any metabolite, regardless of age. In all age groups the average T_2 values of metabolites in the GM are shorter than in the WM by less than 30% for NAA, 16% for Cr, and 10% for Cho, as shown in Table 1 and Fig. 5. The extent of these differences suggests that use of a single set of one T_2 value per metabolite: 343, 172 and 248 ms for NAA, Cr and Cho anywhere in the brain of healthy subjects of any age would impact quantification precision by less than ±10% for *TE*s under 100 ms. For example, neglecting the range of T_2s at *TE* = 35 ms would yield errors of less than 3.6% for NAA, 3.4% for Cr and 3.5% for Cho.

The *intra*-subject variations in these T_2s can be inferred from their coefficient of variation (CV). When obtained with this two-point method it cannot be lower than the instrument noise contribution of 3.6/SNR4 (8,11). (SNR_4 would have been achieved if the entire experiment was spent for 1+3=4 averages at TE_1, $SNR_4=SNR\times\sqrt{4}$). The CVs in a single voxel which represent the instrumental noise contribution, therefore, are $4.7/SNR_4$ ≈5% for NAA, $3.6/SNR_4$ ≈10% for Cr, and $3.8/SNR_4$ ≈13% for Cho (see Fig. 2 in reference (8)) . The observed CVs of the T_2s, estimated from the half-width at half maximum of the respective histograms in Fig. 4, ~35%, 29% and 27% for NAA, Cr and Cho, are combination of instrumental and biological noise. Assuming that these noise sources are independent and therefore, add in quadrature: $CV^2_{total}=CV^2_{biology}+CV^2_{instrument}$, indicates that the biological *intra*-subject T_2s variations are 35%, 27% and 24% for NAA, Cr and Cho.

Based on the reported data we conjecture that quantification precision can be improved by using age-specific metabolite T_2s obtained for GM and WM using a linear approximation,

$$T_2^{\text{metabolite}}=\boldsymbol{A}(\text{ms})+\boldsymbol{B}(\text{ms/year})\times\text{age (years)}. \quad [2]$$

The intercept, ***A***, and slope, ***B***, for each metabolite in either tissue type are derived from and presented in the age versus T_2 plots of Fig. 5. These age-corrections for the T_2s can improve the accuracy of absolute metabolic quantification between the young and elderly compared with the set of a single T_2 per metabolite for both tissue types and all ages proposed above. It is also noteworthy that due to the similarity in the *rates* of T_2 decline with age in the WM and GM, shown in Fig. 5, it is unlikely that they reflect the preferential deposition of iron with age in the GM described in (35).

CONCLUSIONS

The inter- and intra- subject T_2 uniformity found across subjects spanning over six decades substantiates three assumptions frequently made in the past for reasons of expediency: that for T_2 correction in ^{1}H-MRS metabolic quantification a single T_2 value per metabolite is sufficient in *(i)* any brain region, *(ii)* of any healthy subject, and *(iii)* at any age. Despite a (very) gradual (less than 1 ms/year) decrease with age in the T_2s of the three main metabolites and their differences between tissue types, the use of a set of one T_2 per metabolite will yield a precision of better than ±10% in metabolic quantification at intermediate and short, *TE*s≤100 ms. The regional T_2s provided for various tissue types and

the expressions for their age dependence facilitate improvement of the accuracy of quantification approaching it biological variability.

Acknowledgments

We thank Drs. Andrew A. Maudsley of the University of Miami and Brian J. Soher of Duke University for the use of their SITools-FITT spectral modeling software. This work was supported by NIH Grants EB01015, NS050520, NS29029 and NS39135.

References

1. Ross BD, Bluml S. Magnetic resonance Spectroscopy of the human brain. Anat Rec. 2001; 265:54–84. [PubMed: 11323770]
2. Gruetter R, Tkac I. Field mapping without reference scan using asymmetric echo-planar techniques. Magn Reson Med. 2000; 43(2):319–323. [PubMed: 10680699]
3. Soher BJ, Young K, Govindaraju V, Maudsley AA. Automated spectral analysis III: application to in vivo proton MR spectroscopy and spectroscopic imaging. Magn Reson Med. 1998; 40(6):822–831. [PubMed: 9840826]
4. Provencher SW. Automatic quantitation of localized in vivo 1H spectra with LCModel. NMR Biomed. 2001; 14(4):260–264. [PubMed: 11410943]
5. Simmons A, Smail M, Moore E, Williams SC. Serial precision of metabolite peak area ratios and water referenced metabolite peak areas in proton MR spectroscopy of the human brain. Magn Reson Imaging. 1998; 16(3):319–330. [PubMed: 9621973]
6. Dong Z, Dreher W, Leibfritz D. Toward quantitative short-echo-time in vivo proton MR spectroscopy without water suppression. Magn Reson Med. 2006; 55(6):1441–1446. [PubMed: 16598735]
7. Jansen JF, Backes WH, Nicolay K, Kooi ME. 1H MR spectroscopy of the brain: absolute quantification of metabolites. Radiology. 2006; 240(2):318–332. [PubMed: 16864664]
8. Zaaraoui W, Fleysher L, Fleysher R, Liu S, Soher BJ, Gonen O. Human brain-structure resolved T(2) relaxation times of proton metabolites at 3 Tesla. Magn Reson Med. 2007; 57(6):983–989. [PubMed: 17534907]
9. Tsai SY, Posse S, Lin YR, Ko CW, Otazo R, Chung HW, Lin FH. Fast mapping of the T2 relaxation time of cerebral metabolites using proton echo-planar spectroscopic imaging (PEPSI). Magn Reson Med. 2007; 57(5):859–865. [PubMed: 17457864]
10. Fleysher L, Fleysher R, Liu S, Zaaraoui W, Gonen O. Optimizing the precision-per-unit-time of quantitative MR metrics: Examples for T(1), T(2), and DTI. Magn Reson Med. 2007; 57(2):380–387. [PubMed: 17260375]
11. Fleysher R, Fleysher L, Gonen O. The optimal MR acquisition strategy for exponential decay constants estimation. Magn Reson Imaging. 2007
12. Folstein MF, Robins LN, Helzer JE. The Mini-Mental State Examination. Arch Gen Psychiatry. 1983; 40(7):812. [PubMed: 6860082]
13. Reisberg B, Ferris SH, de Leon MJ, Crook T. Global Deterioration Scale (GDS). Psychopharmacol Bull. 1988; 24(4):661–663. [PubMed: 3249768]
14. Reisberg B, Ferris SH. Brief Cognitive Rating Scale (BCRS). Psychopharmacol Bull. 1988; 24(4): 629–636. [PubMed: 3249764]
15. Hu J, Javaid T, Arias-Mendoza F, Liu Z, McNamara R, Brown TR. A fast, reliable, automatic shimming procedure using 1H chemical-shift-imaging spectroscopy. J Magn Reson B. 1995; 108(3):213–219. [PubMed: 7670755]
16. Ogg RJ, Kingsley PB, Taylor JS. WET, a T1- and B1-insensitive water-suppression method for in vivo localized 1H NMR spectroscopy. J Magn Reson B. 1994; 104(1):1–10. [PubMed: 8025810]
17. Bottomley PA. Spatial localization in NMR spectroscopy in vivo. Ann N Y Acad Sci. 1987; 508:333–348. [PubMed: 3326459]

18. Goelman G, Liu S, Hess D, Gonen O. Optimizing the efficiency of high-field multivoxel spectroscopic imaging by multiplexing in space and time. Magn Reson Med. 2006; 56(1):34–40. [PubMed: 16767711]
19. Goelman G, Liu S, Gonen O. Reducing voxel bleed in Hadamard-encoded MRI and MRS. Magn Reson Med. 2006; 55(6):1460–1465. [PubMed: 16685718]
20. Brooker HR, Mareci TH, Mao JT. Selective Fourier transform localization. Magn Reson Med. 1987; 5(5):417–433. [PubMed: 3431402]
21. Mareci T, Brooker H. Essential considerations for spectral localization using indirect gradient encoding of spatial information. J Magn Reson. 1991; 92:229–246.
22. Macovski A. Noise in MRI. Magn Reson Med. 1996; 36(3):494–497. [PubMed: 8875425]
23. Marion D, Ikura M, Bax A. Improved solvent suppression in one- and two-dimensional NMR spectra by convolution of time domain data. J Magn Reson. 1989; 84:425–430.
24. Du YP, Parker DL, Davis WL, Cao G. Reduction of partial-volume artifacts with zero-filled interpolation in three-dimensional MR angiography. J Magn Reson Imaging. 1994; 4(5):733–741. [PubMed: 7981519]
25. Bernstein MA, Fain SB, Riederer SJ. Effect of windowing and zero-filled reconstruction of MRI data on spatial resolution and acquisition strategy. J Magn Reson Imaging. 2001; 14(3):270–280. [PubMed: 11536404]
26. Soher BJ, Young K, Maudsley AA. Representation of strong baseline contributions in 1H MR spectra. Magn Reson Med. 2001; 45(6):966–972. [PubMed: 11378873]
27. Ernst, RR.; Bodenhausen, G.; Wokaun, A. The International Series of Monographs on Chemistry. Oxford: Clarendon Press; 1987. Principles of Nuclear Magnetic Resonance in One and Two Dimensions; p. 152
28. Traber F, Block W, Lamerichs R, Gieseke J, Schild HH. 1H metabolite relaxation times at 3.0 tesla: Measurements of T1 and T2 values in normal brain and determination of regional differences in transverse relaxation. J Magn Reson Imaging. 2004; 19(5):537–545. [PubMed: 15112302]
29. Li BS, Regal J, Gonen O. SNR versus resolution in 3D 1H MRS of the human brain at high magnetic fields. Magn Reson Med. 2001; 46(6):1049–1053. [PubMed: 11746567]
30. Mlynarik V, Gruber S, Moser E. Proton T (1) and T (2) relaxation times of human brain metabolites at 3 Tesla. NMR Biomed. 2001; 14(5):325–331. [PubMed: 11477653]
31. Barker PB, Hearshen DO, Boska MD. Single-voxel proton MRS of the human brain at 1.5 T and 3.0 T. Magn Reson Med. 2001; 45(5):765–769. [PubMed: 11323802]
32. Kemper, TL. Neuroanatomical and neuropathological changes during aging and dementia. Knoefel, MLAaJE., editor. New York: Oxford University Press; 1994. p. 728
33. Peters A. The effects of normal aging on myelin and nerve fibers: a review. J Neurocytol. 2002; 31(8–9):581–593. [PubMed: 14501200]
34. Dickstein DL, Kabaso D, Rocher AB, Luebke JI, Wearne SL, Hof PR. Changes in the structural complexity of the aged brain. Aging Cell. 2007; 6(3):275–284. [PubMed: 17465981]
35. Hallgren B, Sourander P. The effect of age on the non-haemin iron in the human brain. J Neurochem. 1958; 3(1):41–51. [PubMed: 13611557]
36. Brass SD, Chen NK, Mulkern RV, Bakshi R. Magnetic resonance imaging of iron deposition in neurological disorders. Top Magn Reson Imaging. 2006; 17(1):31–40. [PubMed: 17179895]
37. Mitsumori F, Watanabe H, Takaya N, Garwood M. Apparent transverse relaxation rate in human brain varies linearly with tissue iron concentration at 4.7 T. Magn Reson Med. 2007; 58(5):1054–1060. [PubMed: 17969101]

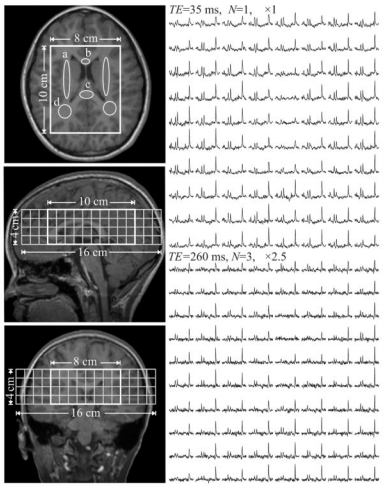

Fig. 1.

Left: Axial, sagittal, and coronal T_1-weighted MRI from an adolescent superimposed with the 8×10×4 cm^3 (LR×AP×IS) VOI and 16×16 cm^2 (LR×AP) axial CSI FOV. Regions of interest (ROI) in the corona radiata (**a**), genu (**b**) and splenium (**c**) of the corpus callosum as well as occipital WM (**d**) are indicated on the axial slice.

Right: Real part of the axial VOI 8×10 (LR×AP) ^{1}H spectra matrix. Top: at TE_1=35 ms, N=1; Bottom: at TE_2= 260 ms, N=3. Spectra are on common horizontal axis (1.7 to 3.7 ppm), but those at TE_2 are all scaled up ×2.5 times for better visualization. Note the SNR and spectral resolution obtained from these 1 cm^3 voxels in 11 and 33 minutes.

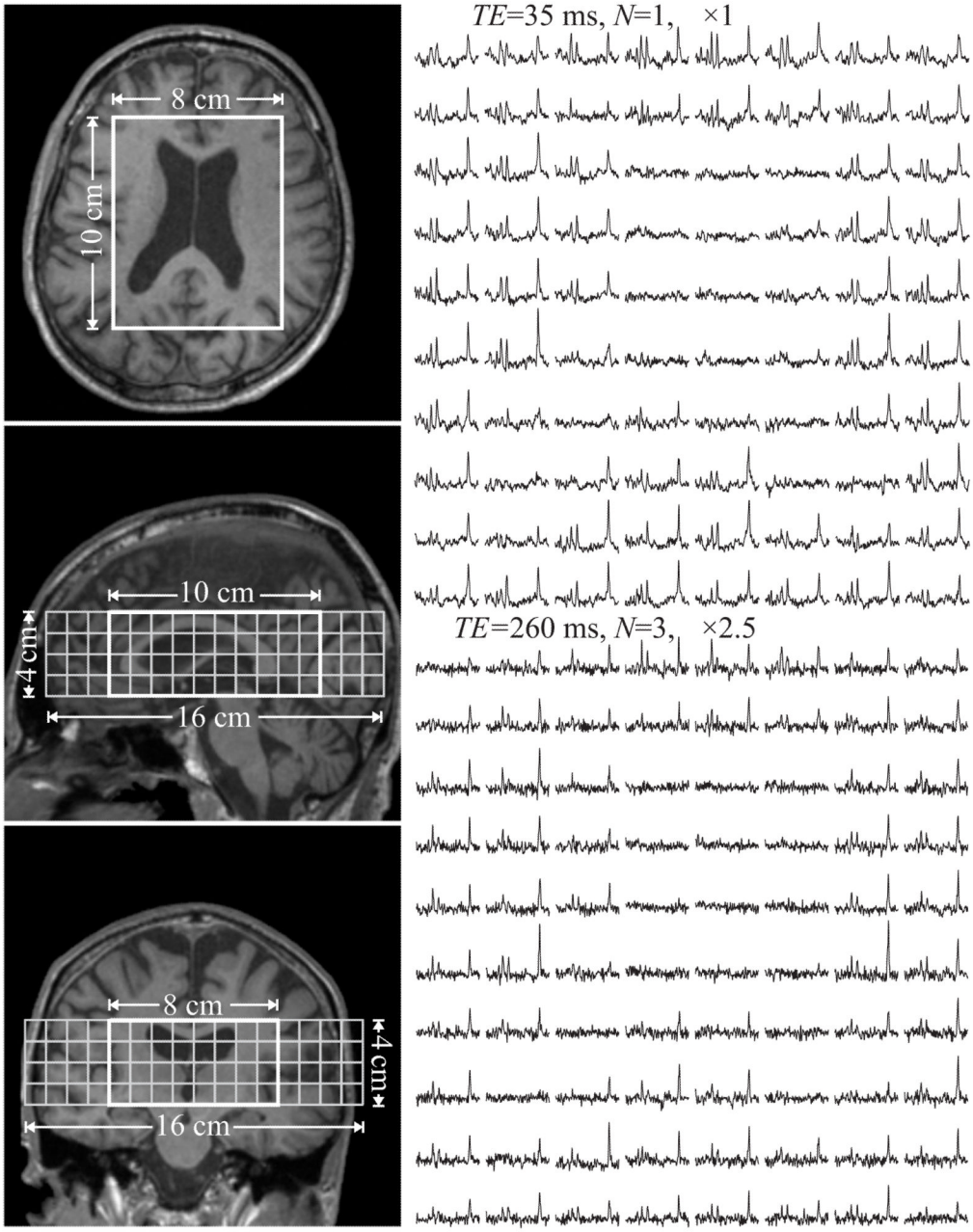

Fig. 2.

Left: Axial, sagittal, and coronal T_1-weighted MRI from an elderly subject superimposed 8×10×4 cm^3 (LR×AP×IS) VOI and 16×16 cm^2 (LR×AP) axial CSI FOV.

Right: Real part of the 8×10 (LR×AP) axial ^1H spectra matrix from the VOI at TE_1=35 ms (N=1) and TE_2=260 ms (N=3). The spectra scales are the same as Fig. 1. Note the SNR and spectral resolution similarity between spectra from elderly and adolescent in comparable anatomical regions (see Fig. 1).

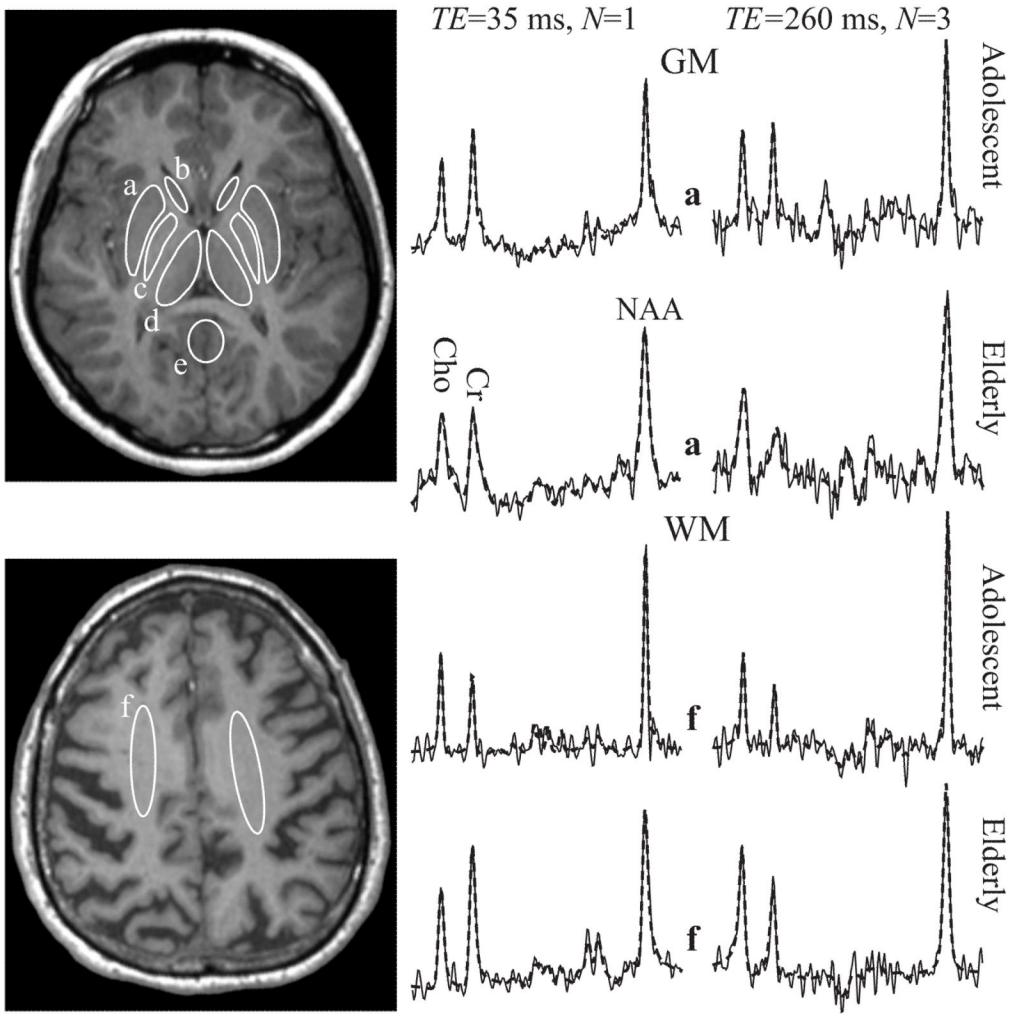

Fig. 3.

Left, top: Axial T_1-weighted image at the basal ganglia level from an adolescent showing the manually outlined GM structure ROIs in the putamen (**a**), caudate (**b**), globus pallidus (**c**), thalamus (**d**) and posterior cingulate gyrus (**e**).

Left, bottom: Axial image of an elderly subject with ROIs in the centrum semiovale (**f**).

Right: GM and WM spectra from the ROIs (**a**) and (**f**) at both *TE*s (solid lines), superimposed with their model functions (dashed lines) fit (3) for NAA, Cr and Cho. Each pair of short and long *TE* spectra is *(i)* from the same subject; and *(ii)* the same voxel within the indicated structure. Note the excellent SNR and fit in all regions and at both *TE*s.

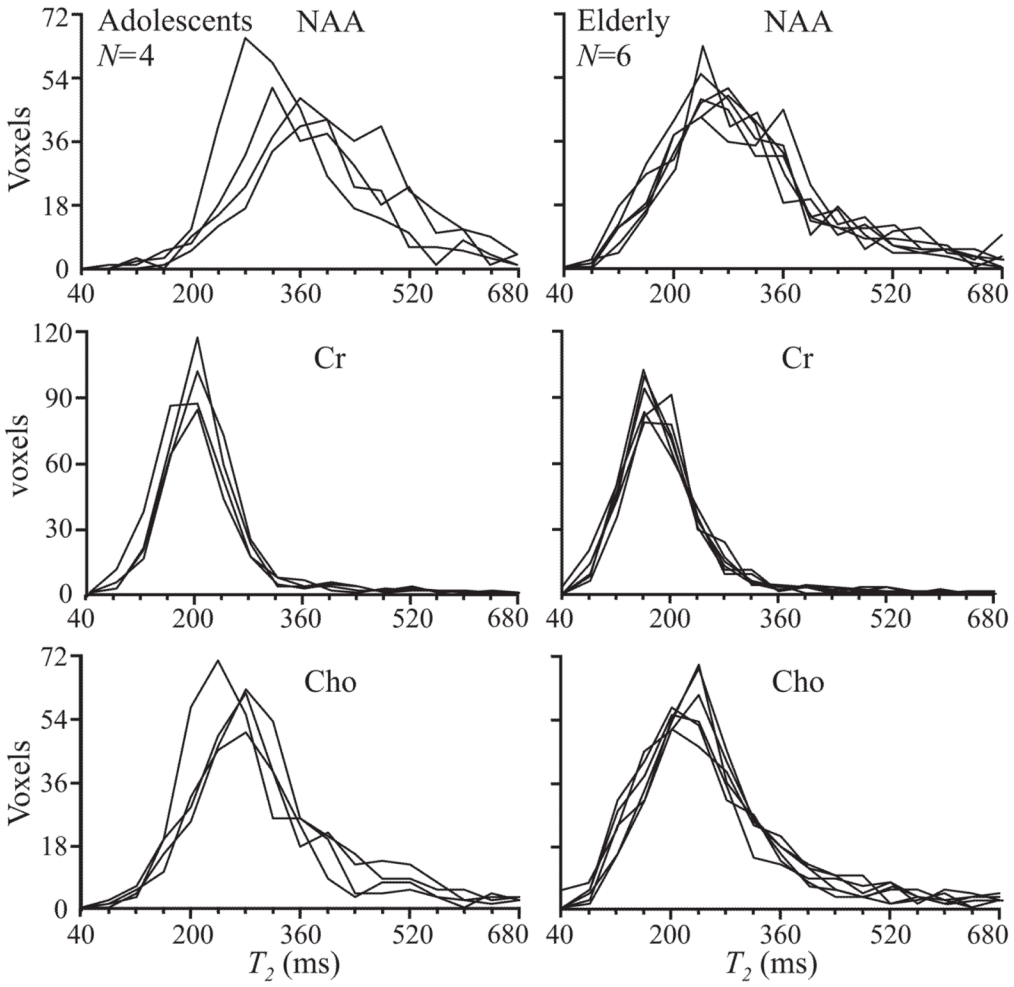

Fig. 4.

Histograms of NAA, Cr and Cho T_2s from all 320 voxels for all the adolescents (N=4) and elderly subjects (N=6). Note that the 60 year age difference does not appear to affect the inter-subject similarity of the respective histograms.

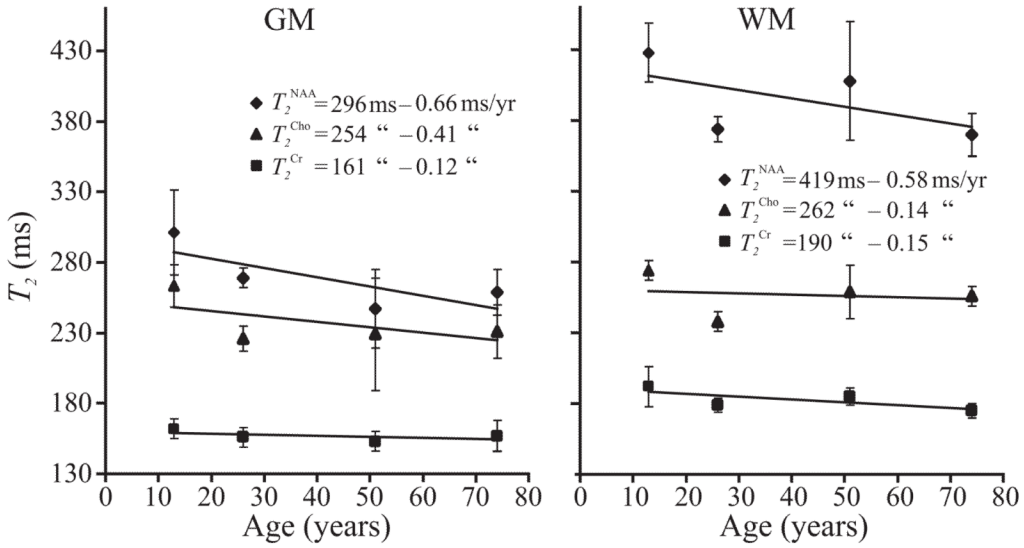

Fig. 5.

Linear fit of age versus T_2 for the NAA, Cr, and Cho in the GM and WM. Error bars represent the SEM. (Data from middle-age subjects (N=2) serves only to rule out significant T_2 non-linearity). Note the age-related T_2 shortening for all metabolites in both GM and WM, which can be accounted for well by a linear fit.

Table 1

Mean values of proton T_2 relaxation times at 3 T (in milliseconds ± SEM) of *N*-acetylaspartate (NAA), creatine (Cr) and choline (Cho) in the various GM and WM brain regions indicated (*cf.* Figs. 1 and 3) in 4 adolescents, 8 young adults, 2 middle-aged, and 6 elderly subjects. CC – corpus callosum.

	T_2 NAA (ms)				T_2 Cr (ms)				T_2 Cho (ms)			
GM:	**Adolescent**	**Young**	**Middle- aged**	**Elderly**	**Adolescent**	**Young**	**Middle- aged**	**Elderly**	**Adolescent**	**Young**	**Middle- aged**	**Elderly**
Caudate	300±23	306±19	203±45	280±33	184±10	194±6	147±36	184±28	258±11	211±4	254±0	240±11
Thalamus	277±13	267±14	288±44	285±15	162±17	152±4	152±4	164±5	268±21	241±12	241±25	235±18
Cingulate gyrus	421±40	277±11	271±9	215±18	162±9	160±5	173±33	147±6	278±18	255±10	324±45	291±26
Globus pallidus	275±5	252±8	219±24	255±8	144±9	141±5	149±27	145±9	240±12	191±11	181±5	206±9
Putamen	310±26	263±13	205±0	223±15	161±9	157±6	151±11	132±9	271±12	216±15	196±2	206±16
GM average	**301±30**	**269±7**	**247±28**	**259±13**	**162±7**	**156±7**	**153±7**	**154±8**	**263±7**	**226±9**	**229±40**	**229±14**
WM:												
Splenium of CC	405±32	375±24	327±19	314±15	205±10	164±4	183±14	193±12	292±9	236±22	207±22	266±31
Genu of CC	361±29	326±21	405±74	310±55	251±36	202±17	175±15	162±10	279±17	247±18	233±26	260±32
Centrum semiovale	458±11	397±16	401±22	391±13	190±2	187±2	186±11	186±7	278±10	245±6	258±22	259±15
Occipital	461±20	366±13	493±81	360±18	188±11	175±5	197±32	169±10	289±21	228±8	272±23	235±16
Corona radiata	400±21	362±21	389±67	383±22	180±7	173±5	180±21	174±8	256±17	234±7	269±43	251±10
WM average	**428±21**	**374±9**	**408±42**	**371±16**	**192±14**	**179±5**	**185±6**	**178±5**	**274±7**	**238±7**	**259±19**	**253±5**
GM+WM	**365±36**	**338±19**	**345±71**	**322±25**	**177±15**	**172±7**	**172±13**	**167±8**	**268±8**	**234±7**	**247±30**	**242±11**
GM+WM average	**343**				**172**				**248**			